Monthly Notices of the ROYAL ASTRONOMICAL SOCIETY

MNRAS **523,** 4431–4440 (2023)
Advance Access publication 2023 June 7

https://doi.org/10.1093/mnras/stad1682

Global transonic solution of hot accretion flow with thermal conduction

Samik Mitra,[1] Sayyedeh Masoumeh Ghoreyshi,[2]★ Amin Mosallanezhad,[3]★ Shahram Abbassi[2] and Santabrata Das [1]★

[1]*Department of Physics, Indian Institute of Technology Guwahati, Guwahati, Assam 781039, India*
[2]*Department of Physics, School of Science, Ferdowsi University of Mashhad, Mashhad, PO Box 91775-1436, Iran*
[3]*School of Mathematics and Statistics, Xi'an Jiaotong University, Xi'an, Shaanxi 710049, China*

Accepted 2023 May 27. Received 2023 May 22; in original form 2023 March 22

ABSTRACT

We examine the effect of thermal conduction on the low-angular momentum hot accretion flow (HAF) around non-rotating black holes accreting mass at very low rate. While doing so, we adopt the conductive heat flux in the saturated form, and solve the set of dynamical equations corresponding to a steady, axisymmetric, viscous, advective accretion flow using numerical methods. We study the dynamical and thermodynamical properties of accreting matter in terms of the input parameters, namely energy (ε_0), angular momentum (ℓ_0), viscosity parameter (α), and saturation constant (Φ_s) regulating the effect of thermal conduction. We find that Φ_s plays a pivotal role in deciding the transonic properties of the global accretion solutions. In general, when Φ_s is increased, the critical point (r_c) is receded away from the black hole, and flow variables are altered particularly in the outer part of the disc. To quantify the physically acceptable range of Φ_s, we compare the global transonic solutions with the self-similar solutions, and observe that the maximum saturation constant (Φ_s^{max}) estimated from the global solutions exceeds the saturated thermal conduction limit (Φ_{sc}) derived from the self-similar formalism. Moreover, we calculate the correlation between α and Φ_s^{max} and find ample disagreement between global solutions and self-similar solutions. Further, using the global flow variables, we compute the Bernoulli parameter (*Be*) which remains positive all throughout the disc, although flow becomes loosely unbound for higher Φ_s. Finally, we indicate the relevance of this work in the astrophysical context in explaining the possibility of mass-loss/outflows from the unbound disc.

Key words: accretion, accretion disc – black hole physics – conduction – hydrodynamics.

1 INTRODUCTION

The accretion of gas onto black holes (BHs) is believed to be one of the primary sources of power for a wide range of active phenomena in our Universe, such as X-ray binaries (XRBs), gamma-ray bursts and active galactic nuclei (AGNs; e.g. Lamb, Lamb & Pines 1973; Treves et al. 1988; Esin, McClintock & Narayan 1997; Fryer, Woosley & Hartmann 1999; Davis, Done & Blaes 2006; Wilkinson & Uttley 2009; Yuan et al. 2010; Veledina, Poutanen & Vurm 2013; Chatterjee et al. 2020). In terms of their temperature, the accreting gas can be classified into two very distinct categories, namely cold and hot accretion flows. The cold accretion flows, commonly explained using either standard thin disc model (Shakura & Sunyaev 1973) and/or the slim disc model (Abramowicz et al. 1988), are radiatively efficient, and remain optically thick. These models are characterized by high mass accretion rate usually exceeds the Eddington limit. Indeed, the cold accretion models with temperatures in the range of 10^4–10^7 K successfully explain the spectrum of luminous AGNs (Liu et al. 2012; Netzer & Trakhtenbrot 2014), black hole X-ray binaries (BH-XRBs) in the high-soft state (Meyer, Liu & Meyer-Hofmeister 2000; Dexter & Quataert 2012), narrow-line Seyfert galaxies (Mineshige et al. 2000; Wang & Netzer 2003; Haba et al. 2008), and ultra-luminous X-ray sources (Watarai, Mizuno & Mineshige 2001; Chen & Wang 2004; Godet et al. 2012; Soria et al. 2015).

On the contrary, in a hot accretion model with a low mass accretion rate, only a small fraction of the energy generated by turbulence is radiated away and most of the thermal energy is stored in the accretion flow, which is then advected into the BH. As a result, the temperature of the gas becomes extremely high although its density and scale height remain smaller in comparison with the well-known standard thin disc (Shakura & Sunyaev 1973). Hot accretion flows (HAFs), the subject of this study, have a drastically reduced radiative efficiency, leading to this model being referred to as a radiatively inefficient accretion flow (Ichimaru 1977; Narayan & Yi 1994; Yuan & Narayan 2014).

It is noteworthy that HAF models successfully explain the observational features of various BH systems including the supermassive BH in our Galactic center (Sgr A∗; Manmoto, Mineshige & Kusunose 1997; Yuan, Markoff & Falcke 2002; Yuan & Narayan 2014), M87 (Reynolds et al. 1996; Park et al. 2019), and the other low-luminosity AGNs (LLAGNs; Lasota et al. 1996; Nemmen et al. 2006; Nemmen, Storchi-Bergmann & Eracleous 2014; Younes et al. 2019), and also BH-XRBs in the hard/quiescence states (Esin et al. 1997; Hameury et al. 1997; Yuan & Cui 2005; Liu, Done & Taam 2011).

One of the most important findings of the numerical simulations is the existence of outflows in HAFs (e.g. Ohsuga et al. 2009; Yuan,

★ E-mail: smghoreyshi64@gmail.com (SMG); mosallanezhad@xjtu.edu.cn (AM); sbdas@iitg.ac.in (SD)

Wu & Bu 2012a; Yuan, Bu & Wu 2012b; Yuan et al. 2015; Bu et al. 2016b, c; Mosallanezhad et al. 2022) that has been confirmed by observation of LLAGNs and XRBs (e.g. Wang et al. 2013; Cheung et al. 2016; Homan et al. 2016; Ma et al. 2019; Park et al. 2019). In the presence of outflows, mass, angular momentum, and energy are removed from the disc, which can have a profound effect on the dynamics and structure of the flow (Yuan et al. 2018; Bu & Yang 2019). Therefore, the modelling of HAFs is able to make the properties of winds/outflows easier. For instance, a recent study of Yang et al. (2021) indicates that a larger BH spin and stronger magnetic fields lead to stronger winds/outflows from the disc.

Taking into account the temperature and density profiles of the HAFs with very low accretion rates, it appears that the collisional mean free paths of the charged particles are much larger than the typical length-scale of accretion flows, i.e. $r_{\rm g} = GM_{\rm BH}/c^2$, where $r_{\rm g}$ is the gravitational radius, and G, $M_{\rm BH}$, and c are the gravitational constant, the BH mass, and speed of light, respectively (Mahadevan & Quataert 1997; Tanaka & Menou 2006; Johnson & Quataert 2007). The plasma in HAFs is, therefore, expected to be collisionless with thermal conduction playing a significant role.

The effect of thermal conduction on the physical properties of HAFs has been explored in several studies based on self-similar assumptions (Tanaka & Menou 2006; Shadmehri 2008; Faghei 2012b; Khajenabi & Shadmehri 2013; Ghoreyshi & Shadmehri 2020; Mosallanezhad et al. 2021). In an early attempt, Tanaka & Menou (2006) reported that thermal conduction in HAFs possibly helps the gas to be launched from the disc as outflows. In addition, the effect of thermal conductivity on the energy flux of outflows as well as the size of the outflowing region appears to be significant (Khajenabi & Shadmehri 2013). Meanwhile, numerical simulations of HAFs indicate that the energy flux carried by the outflows in the presence of thermal conduction can be increased by a factor of $\sim$10 (Bu, Yuan & Stone 2011; Bu, Wu & Yuan 2016a). Further, Narayan & Yi (1995a, b) suggested that the positive Bernoulli parameter is required for outflows to occur in an accretion disc. As a result, the gas becomes gravitationally unbound and escapes from the gravitational potential of the central BH. It is noteworthy that a positive Bernoulli parameter results from the self-similar framework as well (Nakamura 1998; Yuan 1999; Abramowicz, Lasota & Igumenshchev 2000; Yuan et al. 2015).

Although the self-similar solutions provide the physical insights of the accretion flow, they fail to decipher the global behaviour of the accretion flow, especially at the inner and outer disc boundaries (Narayan, Kato & Honma 1997; Chen, Abramowicz & Lasota 1997). Because of this, several authors investigated the global solutions to HAFs around BHs in a self-consistent manner (Abramowicz et al. 1996; Narayan et al. 1997; Chen et al. 1997; Nakamura et al. 1997; Popham & Gammie 1998; Lu, Gu & Yuan 1999; Becker & Le 2003; Chakrabarti & Das 2004; Das 2007; Yuan, Ma & Narayan 2008; Das, Becker & Le 2009; Narayan & Fabian 2011; Kumar & Gu 2018; Kumar & Yuan 2021; Das et al. 2022; Mitra et al. 2022). A pioneering and fascinating study of the global structure and dynamics considering single temperature HAFs was carried out by Narayan et al. (1997). Upon comparing the global and self-similar solutions, they showed that the self-similar solutions satisfactorily mimic the regions avoiding the inner and the outer boundaries of the disc. Due to this, the spectra derived by using the self-similar solutions require modifications, as the swarm of high energy photons originated from the regions near the inner boundary is not accounted appropriately. In addition, Narayan et al. (1997) reported that the global solution leads to a negative Bernoulli parameter in the outer regions of the disc (see also Yuan 1999; Kumar & Gu 2018). Further, Yuan (1999) showed that the outer boundary conditions may significantly affect the value of Bernoulli parameter and its sign, as well. In reality, the Bernoulli parameter depends not only on the outer boundary conditions, but also on factors, such as the viscosity parameter, the adiabatic index, and the advection parameter (Narayan et al. 1997; Popham & Gammie 1998; Narayan & Fabian 2011; Kumar & Gu 2018).

Over the course of accretion, the infall velocity approaches the speed of light when the accreting matter enters the BH (Weinberg 1972), while it becomes negligible at large distances away from the BH horizon (Frank, King & Raine 2002; Das 2007, and references therein). As a result, the accreting gas experiences a subsonic to supersonic transition at a point called the critical point (Liang & Thompson 1980; Abramowicz & Zurek 1981). The critical point depends on the value of the viscosity parameter and the outer boundary conditions (Chakrabarti 1996; Narayan et al. 1997; Yuan 1999; Chakrabarti & Das 2004; Yuan et al. 2008). Moreover, if there are multiple critical points in accretion flows, the flows may undergo shocks (Fukue 1987). The shocked disc may satisfy the observational criteria for the formation of the observed outflows (Das et al. 2001; Becker, Das & Le 2008; Das & Chattopadhyay 2008; Das et al. 2009; Aktar, Das & Nandi 2015; Aktar et al. 2017, 2018). In particular, Das et al. (2009) demonstrated that the existence of shocks relies on the level of viscous dissipation. However, Narayan et al. (1997) examined similar transonic solutions for a wide range of the viscosity parameter, but did not report any shock (see also Chen et al. 1997; Nakamura et al. 1997; Lu et al. 1999; Yuan et al. 2008), possibly due to the choice of selective boundary conditions.

Considering all these, in this work, we intend to examine the three primary objectives concerning the HAFs. First, we aim to investigate the global transonic solutions of HAFs that include thermal conduction. This is particularly relevant for systems with an extremely low mass accretion rate, such as Sgr A$*$ and M87, where the accretion flows are weakly collisional. In such systems, the electron collisional mean free path can be comparable to the typical size of the system, resulting in a significant influence of thermal conduction on the dynamics of the accretion flow and energy transport from the inner to outer regions (Johnson & Quataert 2007; Quataert 2008). Our next objective is to determine the range of the thermal conduction parameter within which the global solutions are viable for the given set of physical input parameters. This is an essential step in our study, as it allows us to identify the critical threshold for thermal conduction for which the global solutions cease to exist. Thirdly, we compare the results of global transonic solutions with the self-similar solutions of HAFs in the presence of thermal conductivity. This analysis provides a more detailed understanding of the impact of thermal conduction on the dynamics of HAFs.

The remainder of the manuscript is organized as follows: In Section 2, the basic equations, physical assumptions, and the boundary conditions are introduced. The numerical results are presented in detail in Section 3. Finally, in Section 4, we provide the discussion and summary of the present work.

2 HOT ACCRETION FLOWS WITH SATURATED THERMAL CONDUCTION

We begin with a low angular momentum steady axisymmetric viscous advective accretion flow around a non-rotating BH. Moreover, we assume that the mass accretion takes place at very low rate representing the radiatively inefficient HAF. In the subsequent

sections, we study the properties of the HAF in the presence of thermal conduction.

2.1 Dynamical equations

In order to deal with the HAF, we adopt a cylindrical coordinate system (r, ϕ, z). We employ the same set of height-integrated governing equations as delineated in Narayan et al. (1997) except the energy equation, where we include the effect of thermal conduction. In addition, we consider the hydrostatic equilibrium in the vertical direction and hence, the flow variables are vertically averaged. Accordingly, in this formulation, the flow variables are expressed as functions of the cylindrical radius r only. Under these assumptions, the governing equations are given by,

$$\dot{M} = -4\pi r H \rho v, \tag{1}$$

$$v\frac{\mathrm{d}v}{\mathrm{d}r} = (\Omega^2 - \Omega_{\rm K}^2)r - \frac{1}{\rho}\frac{\mathrm{d}(\rho C_{\rm s}^2)}{\mathrm{d}r}, \tag{2}$$

$$\rho r H v \frac{\mathrm{d}(\Omega r^2)}{\mathrm{d}r} = \frac{\mathrm{d}}{\mathrm{d}r}\left(\nu\rho H r^3 \frac{\mathrm{d}\Omega}{\mathrm{d}r}\right), \tag{3}$$

$$\frac{\rho v}{(\gamma-1)}\frac{\mathrm{d}C_{\rm s}^2}{\mathrm{d}r} - C_{\rm s}^2 v\frac{\mathrm{d}\rho}{\mathrm{d}r} = f\nu\rho r^2\left(\frac{\mathrm{d}\Omega}{\mathrm{d}r}\right)^2 - \frac{1}{r}\frac{\mathrm{d}(rF_{\rm s})}{\mathrm{d}r}. \tag{4}$$

In the above equations, ρ and Ω are the mass density and the angular velocity of the gas, respectively. The radial velocity of the flow v is assumed to be negative for an inward flow of gas. Here, $H \equiv C_{\rm s}/\Omega_{\rm K}$ is the vertical half-thickness of the flow, where $C_{\rm s}$ is the isothermal sound speed and $\Omega_{\rm K}$ is the Keplerian angular velocity. Adopting pseudo-Newtonian potential $\Psi = -GM_{\rm BH}/(r - r_{\rm s})$ (Paczyński & Wiita 1980), the Keplerian angular velocity is given by,

$$\Omega_{\rm K}^2 = \frac{GM_{\rm BH}}{r(r-r_{\rm s})^2}, \tag{5}$$

where $r_{\rm s} = 2GM_{\rm BH}/c^2$ is the Schwarzschild radius for a BH with mass $M_{\rm BH}$. The last term on the right-hand side of equation (2) is the acceleration due to the pressure gradient. Here, the pressure is defined by the isothermal sound speed $C_{\rm s}$ and the density ρ as $p = \rho C_{\rm s}^2$. A Shakura–Sunyaev prescription (Shakura & Sunyaev 1973) is adopted for the kinematic coefficient of viscosity (ν) as,

$$\nu = \alpha C_{\rm s} H, \tag{6}$$

where α is the viscosity parameter. We assume that the viscosity parameter is a constant, and is independent of r. By substituting equation (6) into equation (3), and using equation (1), we have,

$$\frac{\mathrm{d}}{\mathrm{d}r}\left(\rho H v r^3 \Omega\right) = \frac{\mathrm{d}}{\mathrm{d}r}\left(\frac{\alpha C_{\rm s}^2 \rho H r^3}{\Omega_{\rm K}}\frac{\mathrm{d}\Omega}{\mathrm{d}r}\right), \tag{7}$$

which on integration gives

$$\frac{\mathrm{d}\Omega}{\mathrm{d}r} = \frac{v\Omega_{\rm K}(\ell - \ell_0)}{\alpha r^2 C_{\rm s}^2}, \tag{8}$$

where $\ell = \Omega r^2$ is the angular momentum per unit mass (hereafter specific angular momentum) for the accreting gas at radius r. The integration constant ℓ_0 represents the specific angular momentum eventually swallowed by the BH. In energy equation (4), γ is the ratio of specific heats of the gas. The advection parameter f (= 1 − $Q_{\rm rad}/Q_{\rm vis}$) is assumed to be a constant which lies in the range $0 \le f \le 1$. Here, $Q_{\rm vis}$ and $Q_{\rm rad}$ denote viscous heating and radiative cooling rates. Since the collisional mean free paths of the charged particles in HAFs are much larger than the typical length-scale of the accretion flows, one may no longer apply the classical theory for thermal conduction. Under these conditions, the heat flux is described as the saturated form of conduction. The last term on right-hand side of equation (4) represents the transfer of energy due to the saturated thermal conduction. Following Cowie & McKee (1977), the saturated conduction flux $F_{\rm s}$ is obtained as,

$$F_{\rm s} = 5\Phi_{\rm s}\rho C_{\rm s}^3, \tag{9}$$

where $\Phi_{\rm s}$ is the dimensionless saturation constant with $0 \le \Phi_{\rm s} < 1$. It is noteworthy that the self-similar solutions describing the accretion flow tend to become non-rotating ($\Omega \to 0$) when the saturation constant ($\Phi_{\rm s}$) reaches its limiting value ($\Phi_{\rm sc}$; Shadmehri 2008; Ghasemnezhad, Khajavi & Abbassi 2012; Faghei 2012a; Ghoreyshi & Shadmehri 2020). Accordingly, the physically acceptable accretion solutions around a BH are given by the remaining allowed range of the saturation constant, $0 \le \Phi_{\rm s} \le \Phi_{\rm sc}$.

2.2 Critical point and boundary conditions

Using equations (1), (4), (8), and (9), we get the radial gradient of the sound speed as,

$$\left(\frac{\gamma+1}{\gamma-1} + 10\,\Phi_{\rm s}\frac{C_{\rm s}}{v}\right)\frac{\mathrm{d}\ln C_{\rm s}}{\mathrm{d}r} = -\left(1 - 5\Phi_{\rm s}\frac{C_{\rm s}}{v}\right)\frac{\mathrm{d}\ln|v|}{\mathrm{d}r} + \left(1 - 5\Phi_{\rm s}\frac{C_{\rm s}}{v}\right)\frac{\mathrm{d}\ln\Omega_{\rm K}}{\mathrm{d}r} - \frac{1}{r} + \frac{f v\Omega_K}{\alpha r^2 C_{\rm s}^4}(\ell - \ell_0)^2. \tag{10}$$

We next use equations (1) and (10) to eliminate $\mathrm{d}\rho/\mathrm{d}r$ and $\mathrm{d}C_{\rm s}/\mathrm{d}r$ in equation (2) and thereby express the differential dynamical equation as,

$$\left[\frac{2\gamma + 5\,\Phi_{\rm s}(\gamma-1)C_{\rm s}/v}{(\gamma+1) + 10\,\Phi_{\rm s}(\gamma-1)C_{\rm s}/v} - \frac{v^2}{C_{\rm s}^2}\right]\frac{\mathrm{d}\ln|v|}{\mathrm{d}r} = \frac{r\left(\Omega_{\rm K}^2 - \Omega^2\right)}{C_{\rm s}^2} - \left[\frac{2\gamma + 10\,\Phi_{\rm s}(\gamma-1)C_{\rm s}/v}{(\gamma+1) + 10\,\Phi_{\rm s}(\gamma-1)C_{\rm s}/v}\right]\frac{1}{r} + \left[\frac{2\gamma + 5\,\Phi_{\rm s}(\gamma-1)C_{\rm s}/v}{(\gamma+1) + 10\,\Phi_{\rm s}(\gamma-1)C_{\rm s}/v}\right]\frac{\mathrm{d}\ln\Omega_{\rm K}}{\mathrm{d}r} + \frac{f\Omega_{\rm K}v}{\alpha r^2 C_{\rm s}^4} \times \left[\frac{\gamma-1}{(\gamma+1) + 10\,\Phi_{\rm s}(\gamma-1)C_{\rm s}/v}\right](\ell - \ell_0)^2. \tag{11}$$

We numerically solve the differential equations (8), (10), and (11) to obtain the radial profile of v, $C_{\rm s}$ and ℓ. In doing so, one requires to supply the boundary conditions. As stated in the introduction, the inflowing gas starts its journey from the outer edge of the disc with negligible radial velocity ($|v| \ll c$, i.e. subsonic). However, the matter flows into the BH with supersonic velocity ($|v| \sim c$) to satisfy the inner boundary conditions imposed by the event horizon. Therefore, the flow must change its sonic state at the critical point ($r_{\rm c}$) to become transonic at least once, if not multiple times. At the critical point, the radial velocity gradient takes the form $\mathrm{d}v/\mathrm{d}r|_{\rm c} = 0/0$ as both numerator $\mathcal{N}_{\rm c}$ and denominator $\mathcal{D}_{\rm c}$ simultaneously vanish at $r_{\rm c}$, and we have the critical point conditions $\mathcal{N}_{\rm c} = \mathcal{D}_{\rm c} = 0$, which are explicitly yielded as,

$$\mathcal{D}_{\rm c} \equiv \frac{2\gamma + 5\,\Phi_{\rm s}(\gamma-1)C_{\rm sc}/v_{\rm c}}{(\gamma+1) + 10\,\Phi_{\rm s}(\gamma-1)C_{\rm sc}/v_{\rm c}} - \frac{v_{\rm c}^2}{C_{\rm sc}^2} = 0, \tag{12}$$

$$\mathcal{N}_{\rm c} \equiv \frac{r_{\rm c}\left(\Omega_{\rm K}^2 - \Omega_{\rm c}^2\right)}{C_{\rm sc}^2} - \left[\frac{2\gamma + 10\,\Phi_{\rm s}(\gamma-1)C_{\rm sc}/v_{\rm c}}{(\gamma+1) + 10\,\Phi_{\rm s}(\gamma-1)C_{\rm sc}/v_{\rm c}}\right]\frac{1}{r_{\rm c}} + \left[\frac{2\gamma + 5\,\Phi_{\rm s}(\gamma-1)C_{\rm sc}/v_{\rm c}}{(\gamma+1) + 10\,\Phi_{\rm s}(\gamma-1)C_{\rm sc}/v_{\rm c}}\right]\frac{\mathrm{d}\ln\Omega_{\rm K}}{\mathrm{d}r} + \frac{f\Omega_{\rm K}v_{\rm c}}{\alpha r_{\rm c}^2 C_{\rm sc}^4} \times \left[\frac{\gamma-1}{(\gamma+1) + 10\,\Phi_{\rm s}(\gamma-1)C_{\rm sc}/v_{\rm c}}\right](\ell_{\rm c} - \ell_0)^2 = 0, \tag{13}$$

where v_c, Ω_c, C_{sc}, and ℓ_c denote the radial and the angular velocities, sound speed, and the angular momentum at the critical point (r_c), respectively. Since the flow remains smooth along the streamline, dv/dr must be real and finite all throughout. Hence, we calculate $dv/dr|_c$ by applying the L'Hôpital's rule, leading to

$$\left(\frac{dv}{dr}\right)_c = \left(\frac{d\mathcal{N}/dr}{d\mathcal{D}/dr}\right)_{r=r_c}. \tag{14}$$

In general, $dv/dr|_c$ possesses two distinct values at r_c. When both values of $dv/dr|_c$ are real and of opposite sign, i.e. $dv/dr|_c < 0$, and $dv/dr|_c > 0$, we obtain saddle type critical points (Das 2007; Das et al. 2009; Mitra et al. 2022, and references therein). Note that saddle type critical points are of special interest as the global transonic accretion flow has to pass through it (Chakrabarti & Das 2004).

Another boundary condition implies the vanishing of the viscous shear stress at the horizon (Becker & Le 2003; Das et al. 2009). Hence, considering $d\Omega/dr = 0$, we obtain,

$$\lim_{r\to r_s} \Omega(r) \equiv \Omega_0 = \frac{\ell_0}{r_s^2}. \tag{15}$$

Applying the aforementioned conditions and adopting the methodology outlined in the following subsection, we obtain the comprehensive global transonic accretion solutions around BHs in the presence of thermal conduction. With careful adherence to this approach, we can accurately model the behaviour and characteristics of the accretion flow that provide the precious insights into the underlying physical processes under considerations.

2.3 Globally conserved energy equation

In order to obtain the energy transport rate per unit mass of a viscous advective flow in the presence of thermal conduction, we rewrite equation (4) as

$$\mathcal{E} = \frac{v^2}{2} - \frac{\ell^2}{2r^2} + \Psi + h + \frac{\ell\ell_0}{r^2} + \frac{5\Phi_s C_s^3}{v} - \int \left(\frac{5\Phi_s C_s^3}{vH}\frac{dH}{dr}\right) dr, \tag{16}$$

where h [$= \gamma p/\rho(\gamma - 1)$] is the specific enthalpy. We note that the saturated conduction flux decreases in regions of the accreting flow where the electrons become relativistic (Tanaka & Menou 2006). Therefore, the effect of thermal conduction can be negligible in the inner regions (r_{in}) of the disc. Accordingly, we set $\Phi_s \sim 0$ at r_{in}, and redefine the energy transport rate per unit mass (ε_0) at r_{in} as

$$\varepsilon_0 = \frac{v^2}{2} - \frac{\ell^2}{2r^2} + \Psi + h + \frac{\ell\ell_0}{r^2}. \tag{17}$$

We fix the energy ε_0 at r_{in} and obtain the global solutions following the methodology as delineated in Appendix A. It is important to note that ε_0 is conserved for a viscous advective accretion flow. Moreover, we express the Bernoulli parameter (Be; Nakamura et al. 1997) that contains the local information of radial motion, azimuthal motion, gravity, and thermodynamic terms, and is given by,

$$Be = \frac{v^2}{2} + \frac{\ell^2}{2r^2} + \Psi + h. \tag{18}$$

Needless to mention that in absence of any viscosity, $\ell = \ell_0$ and hence, we have $\varepsilon_0 = Be$.

3 NUMERICAL RESULTS

In obtaining the accretion solutions, we employ a unit system with $GM_{BH} = c = 1$. This allows us to simplify our calculations and obtain results that are seamlessly compared with previous studies. The structure of HAFs is influenced by a variety of factors, including the energy transport rate ε_0 at r_{in}, angular momentum transport rate ℓ_0 at the horizon, the viscosity parameter α, the saturation constant Φ_s, and the ratio of specific heats, γ. In this study, we choose $\gamma = 1.5$ unless stated otherwise, and set $f = 1$ for the purpose of representation. To find the critical point location, we utilize the iteration methodology as described in Becker & Le (2003), Das et al. (2009), and Kumar & Gu (2018) (see Appendix A for more details). We then solve the coupled differential equations (8), (10), and (11) simultaneously for a given set of input parameters (ε_0, ℓ_0, α, Φ_s) to obtain the global solution for HAFs in the presence of thermal conduction. This approach allows us to accurately model the behaviour of HAFs and gain insights into the complex processes that govern their structure.

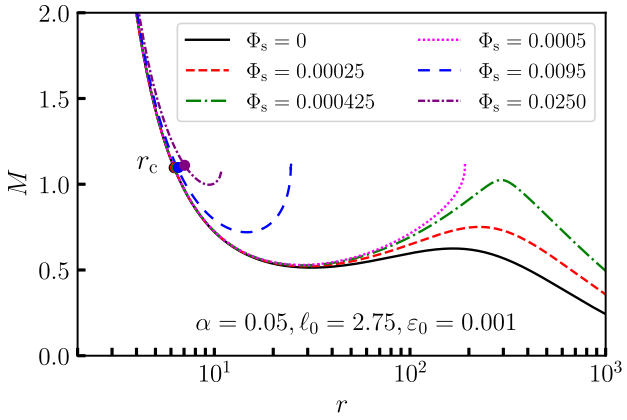

Figure 1. Variation of Mach number ($M = |v|/C_s$) as a function of radial coordinate (r) for different Φ_s values starting from 0 to 0.0250 which are marked. Here, the input parameters are chosen as (ε_0, ℓ_0, α) = (0.001, 2.75, 0.05). The filled circles represent the critical points. See text for the details.

3.1 Global transonic solutions

We choose a set of input parameters, $(\varepsilon_0, \ell_0, \alpha) = (0.001, 2.75, 0.05)$, and integrate the flow equations (8, 10, 11) towards the outer edge (r_{edge}) of the disc starting from $r_{in} = 2.001$ considering $\Phi_s = 0$. The obtained results are depicted in Fig. 1, where the solid (black) curve smoothly connects the horizon with $r_{edge} = 1000$ via a critical point at $r_c = 6.233$. Solutions of this kind where a subsonic flow ($v \ll c$) from a large distance smoothly crosses the BH horizon supersonically are called global accretion solutions. Next, we increase the saturation constant to $\Phi_s = 0.000\,25$, and notice that the obtained global solution (dashed curve in red) deviates from the global solution with $\Phi_s = 0$. It is interesting to note that the global accretion solutions obtained for different Φ_s remain quite insensitive, particularly in the inner regions of the disc. However, the effect of thermal conduction on the accretion solutions is prominently visible in the region far from the BH horizon. We keep increasing the saturation constant to a critical value $\Phi_s = 0.000\,425$ (dot–dashed curve in green), beyond that the flow fails to connect the outer edge as the solution becomes closed (Sarkar, Das & Mandal 2018), shown using a dotted (magenta) curve. If we keep increasing Φ_s, we continue to obtain closed solutions depicted in long-dashed (blue) and dot–dashed (purple) curves. Note that these solutions are apparently unphysical unless they join via shock with other solutions passing through another critical point usually located far away from the horizon (Fukue 1987; Chakrabarti 1989, 1996; Das et al. 2001; Chakrabarti & Das 2004; Das 2007;

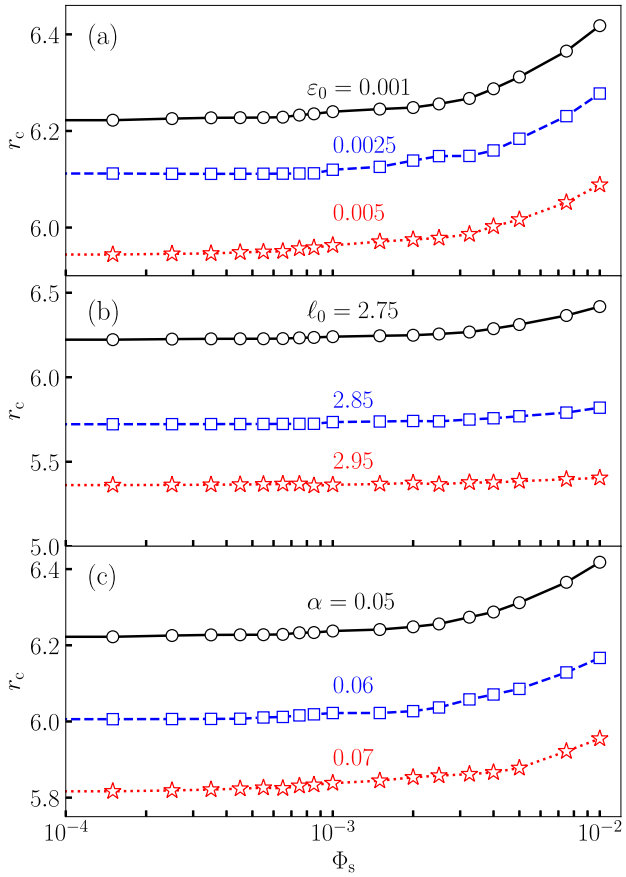

Figure 2. Variation of the critical point location (r_c) as a function of Φ_s. In panel (a), we fix (α, ℓ_0) = (0.05, 2.75), and show r_c for ε_0 = 0.001, 0.0025, and 0.005. In panel (b), we choose (ε_0, α) = (0.001, 0.05), and obtain results for different values of the angular momentum at the horizon as ℓ_0 = 2.75, 2.85, and 2.95. In panel (c), we set (ε_0, ℓ_0) = (0.001, 2.75), and vary the viscosity parameter as α = 0.05, 0.06, and 0.07. In each panel, open circles, squares, and asterisks represent the location of critical points r_c. See text for the details.

Das et al. 2009; Das et al. 2022, and references therein). Finally, we find an upper limit of the saturation constant, $\Phi_s = 0.025$, above which accretion solutions cease. We observe that the critical point shifts outwards when increasing the saturation constant (see Section 3.2). This finding contradicts the previously reported results (Faghei 2012b) and hence, we intend to analyse this in detail in the following Subsection 3.2.

3.2 Dependency of critical point on input parameters

In Fig. 2, we find a unique correspondence between the critical point location and the saturation constant (Φ_s) for different combinations of (ε_0, ℓ_0, α). In Fig. 2a, we choose (ε_0, ℓ_0, α) = (0.001, 2.75, 0.05), and start with $\Phi_s = 0$. For this configuration, we obtain the critical point at $r_c = 6.233$, and as Φ_s is increased, the critical point shifts outwards. In reality, as Φ_s is increased, the flow temperature at a given radial coordinate is decreased (see Fig. 3 b for more details), and hence, C_s is also decreased there. Further, since Mach number M_{r_c} [$= (v/C_s)_{r_c}$] at r_c remains largely insensitive to Φ_s, r_c shifts outward with the increase of Φ_s to restore M_{r_c}. This result is shown using open circles joined using solid (black) lines. Next, we keep (ℓ_0, α) fixed, and increase energy to ε_0 = 0.0025 and 0.005

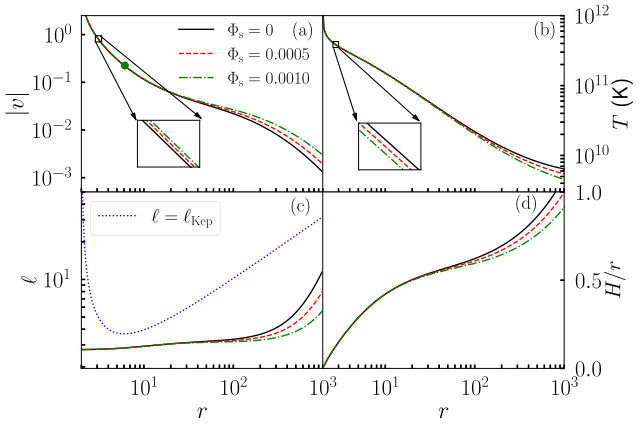

Figure 3. The profiles of velocity v, temperature T, angular momentum ℓ, and aspect ratio H/r are plotted as a function of radial distance r for different values of $\Phi_s = 0$ (solid), 0.0005 (dashed), and 0.0010 (dot–dashed), respectively. Here, the input parameters are chosen as (ε_0, ℓ_0, α) = (0.0025, 2.75, 0.05). See text for the details.

that causes the critical point location to reduce (see open squares in blue and open asterisks in red). Indeed, as energy is increased, the temperature of the disc is also increased, which causes the critical points to move inwards to maintain the higher temperature. In Fig. 2b, we fix (ε_0, α) = (0.001, 0.05) and vary angular momentum as ℓ_0 = 2.75, 2.85, and 2.95, respectively. Finally, in Fig. 2c, we only vary the viscosity parameter as α = 0.05, 0.06, and 0.07 keeping other parameters fixed. When ℓ_0 or α is increased, the frictional force increases within the flow that eventually yielding enhanced viscous heating. Hence, the critical points move inwards with the increase of ℓ_0 or α, although we observe an anti-correlation between Φ_s and any one of the global input parameters, namely ε_0, ℓ_0, and α, over the variation of r_c. However, the overall variation of the critical point location (r_c) with ε_0, ℓ_0, and α appears to remain similar as was reported earlier (Chakrabarti & Das 2004; Das et al. 2009; Das et al. 2022; Mitra et al. 2022).

3.3 The effect of thermal conduction on flow variables

In Fig. 3, we depict the behaviour of flow variables corresponding to the global transonic solutions in the presence of thermal conduction. Here, we set the input parameters as (ε_0, ℓ_0, α) = (0.0025, 2.75, 0.05). The solutions are illustrated for different values of the saturation constant as Φ_s = 0.0, 0.0005, and 0.0010, which are plotted using solid (black), dashed (red), and dot–dashed (green) curves, respectively. In panel (a), the subsonic accretion flow from r_{edge} = 1000 starts accreting with negligible velocity and gradually gains radial velocity as it proceeds towards the BH. At r_c, flow becomes supersonic and ultimately crosses the horizon supersonically. Note that flow velocity exceeds the speed of light just outside the horizon. This happens due to the limitation of the pseudo-Newtonian potential which deviates to mimic the space-time geometry of the BH there. For Φ_s = 0.0, 0.0005, and 0.0010, the critical points are obtained at r_c = 6.0924, 6.1113, and 6.1219, respectively. We find that radial velocity is increased marginally with Φ_s at the inner part of the disc shown at the inset, however, noticeably deviation is observed towards the outer part of the disc. In a convergent flow, the temperature (T) is increased with the decrease of r mainly due to the geometrical compression. However, the presence of thermal conduction generally leads to the reduction of temperature, because the heat generated by the viscous dissipation is transferred away due to the thermal conduction. As

expected, the reduction of temperature at the outer edge of the disc is observed (see panel b of Fig. 3), which are in agreement with the results of the numerical simulation (Wu, Yuan & Bu 2010). In panel (c), we display the variation of the angular momentum ℓ with r corresponding to the solutions presented in panel (a). We find that the angular momentum transport is very inefficient particularly at the inner part of the disc, although the increase of ℓ is seen at higher radial coordinates. Meanwhile, Faghei (2012b) argued that for enhanced Φ_s, viscous turbulence is reduced that weakens the efficiency of angular momentum transport inside the disc. We further compare the flow angular momentum profile with the Keplerian angular momentum ($\ell_{\rm Kep}$) distribution (dotted curve in blue) and observe that ℓ of HAFs remains sub-Keplerian all throughout. In panel (d), we demonstrate the relative thickness of the disc H/r at all radii. From the figure, it is clear that $H/r \ll 1$ is generally maintained at the inner region; however, the flow is intended to become quasi-spherical $H/r \sim 1$ towards the outer regions. Moreover, we find that the disc thickness is reduced in the outer regions as the influence of thermal conduction is increased. This is naturally expected, as the increased Φ_s generally reduces the disc temperature (T) at the outer part of the disc that eventually resulted the reduction of the disc height.

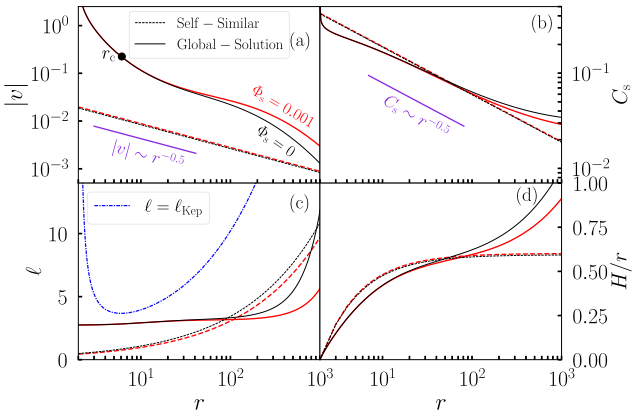

Figure 4. Comparison of the global (solid curves) and self-similar (dashed curves) solutions in the presence and absence of thermal conduction. In panels (a), (b), (c), and (d), radial velocity ($|v|$), sound speed (C_s), angular momentum (ℓ), and local disc thickness (H/r) are plotted, respectively. Here, we choose the input parameters for the global solutions as (ε_0, ℓ_0, α) = (0.0025, 2.75, 0.05; same as in Fig. 3). The thin and thick curves represent results for $\Phi_s = 0$ and $\Phi_s = 0.001$, respectively. For the self-similar solutions, we choose $f = 1$ and $\gamma = 1.5$. See text for the details.

3.4 Self-similar solutions

In this paper, our main objective is to study the global transonic solutions of HAFs in the presence of thermal conduction. In addition, we also intend to conduct a comparative analysis of HAFs by means of the self-similar solutions (Narayan & Yi 1994). These analyses provide the valuable insights of the similarities and differences between the two solutions. Indeed, the self-similar solutions satisfactorily describe the structure of an accretion flow far from boundaries and hence, such solutions are obtained for $r \gg r_s$ that reduces the pseudo-Newtonian potential in the Newtonian form. Following Narayan & Yi (1994), we choose the self-similar treatment in the following forms

$$v(r) = -\alpha C_1 v_{\rm K}, \tag{19}$$

$$\Omega(r) = C_2 \Omega_{\rm K}, \tag{20}$$

$$C_s^2(r) = C_3 v_{\rm K}^2, \tag{21}$$

where $v_{\rm K}$ ($= \sqrt{GM_{\rm BH}/r}$, $G = M_{\rm BH} = 1$) is the Keplerian velocity, and C_1, C_2, and C_3 are constants. By substituting the self-similar solutions (equations 19, 20, 21) into the equations (2)–(4), we obtain a closed set of dimensionless equations that allow us to determine the constants C_1, C_2, and C_3. The closed set of dimensionless equations are given by,

$$-\frac{1}{2}\alpha^2 {C_1}^2 = {C_2}^2 - 1 + \frac{5}{2}C_3, \tag{22}$$

$$C_1 = \frac{3}{2}C_3, \tag{23}$$

$$\left[\frac{1}{\gamma - 1} - \frac{3}{2}\right] C_1 = \frac{9}{4} f {C_2}^2 + 10\frac{\Phi_s}{\alpha}\sqrt{C_3}. \tag{24}$$

After some algebraic manipulations, an equation for C_1 is obtained as

$$\frac{9f\alpha^2}{8}{C_1}^2 + \left[\frac{1}{\gamma - 1} - \frac{3}{2} + \frac{15f}{4}\right] C_1 - \frac{10\sqrt{6}\Phi_s}{3\alpha}\sqrt{C_1} - \frac{9f}{4} = 0. \tag{25}$$

As reported in Tanaka & Menou (2006), that the solution of equation (25) yields the significant changes in the radial and rotational velocity profiles when thermal conduction is active inside the flow. In particular, they pointed out that in the presence of thermal conduction, the accreting flow rotates with lower rate, while its inward motion becomes faster. Meanwhile, we mentioned in Section 2.1 that the accreting flow reaches a non-rotating limit at a specific saturation constant $\Phi_{\rm sc}$. Accordingly, we calculate $\Phi_{\rm sc}$ using equations (22)–(24) subject to the condition $C_2 = 0$. With this, we have

$$\Phi_{\rm sc} = \sqrt{-10 + 2\sqrt{18\alpha^2 + 25}}\,\frac{5 - 3\gamma}{40(\gamma - 1)}. \tag{26}$$

Equation (26) clearly indicates that $\Phi_{\rm sc}$ strictly depends on both viscosity parameter α and ratio of specific heats γ, when self-similar solutions are adopted. What is more is that for $\Phi_s > \Phi_{\rm sc}$, ${C_2}^2$ in equation (24) becomes negative resulting unphysical solutions as it leads to $\Omega^2 < 0$.

In Fig. 4, we compare the global transonic solutions with the self-similar solutions. While doing so, we choose the same set of input parameters for the global solutions as used in Fig. 3, i.e. (ε_0, ℓ_0, α) = (0.0025, 2.75, 0.05). And, for the self-similar solutions, we use $\alpha = 0.05$, $f = 1$, and $\gamma = 1.5$, respectively. In panel (a), the profile of the radial velocity $|v|$ is presented and in panel (b), we show the variation of sound speed C_s. For the self-similar solutions, the effects of thermal conduction on $|v|$, and C_s appear to be insignificant even for high saturation constant $\Phi_s = 0.001$. This happens because both radial velocity and sound speed follow simple power law as $|v|$, $C_s \sim r^{-1/2}$ having ignorable impact of thermal conduction. On the contrary, the impact of Φ_s is seen to be prominent on the global solutions. In addition, the Mach number M ($= |v|/C_s$) in global solutions generally decreases with radius, whereas it remains independent on r for self-similar solutions (Faghei 2012b). In fact, self-similar solutions do not possess critical point as they remain subsonic across the length-scale of the disc. In panel (c), we illustrate the variation of angular momentum ℓ for the same solutions presented in Fig. 4(a). We find that ℓ is reduced with the increase of saturation constant Φ_s particularly towards the outer part of the disc, which is in agreement with the results of Tanaka & Menou (2006). Moreover, ℓ steeply rises

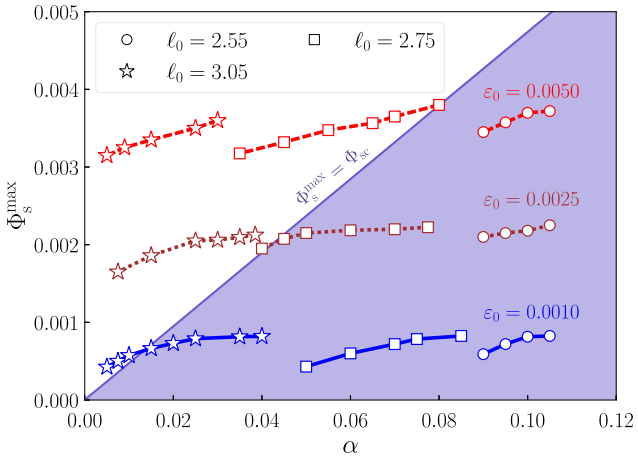

Figure 5. Correlation between α and maximum value of saturation constant Φ_s^{max} that renders the global transonic accretion solutions around BHs. Here, circles, squares, and asterisks are for $\ell_0 = 2.55$, 2.75, and 3.05 and these points connected with solid (blue), dotted (maroon), and dashed (red) lines represent the results for $\varepsilon_0 = 0.0010$, 0.0025, and 0.0050, respectively. The shaded (violet) region corresponds to the self-similar solutions (see equation 26) where slanting solid line refers the limiting value of saturation constant ($\Phi_s^{max} = \Phi_{sc}$). See text for the details.

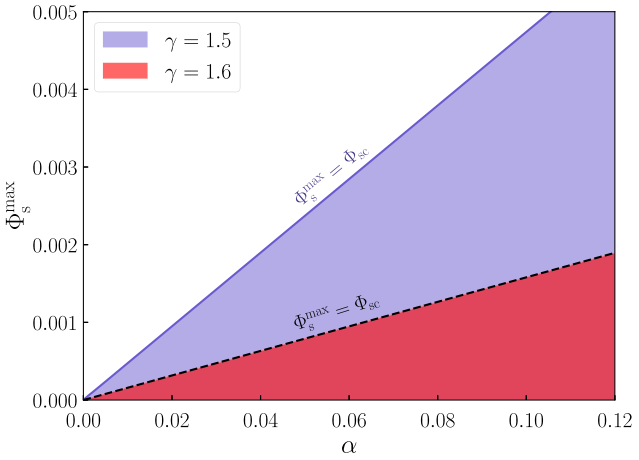

Figure 6. Correlation between α and Φ_s^{max} based on self-similar solutions (see equation 26) for different values of the adiabatic index γ. The shaded region in violet and red are for $\gamma = 1.5$ and 1.6, respectively. See text for the details.

at larger radii as $\ell \propto r^{1/2}$ in self-similar approach, although HAFs remain sub-Keplerian all throughout provided α does not assume high end values. In panel (d), we present the variation of the local disc thickness H/r as a function of r. We observe that in the self-similar model, H/r remains almost constant ($H/r \sim 0.6$) in the outer regions of the disc, whereas flow geometry becomes quasi-spherical ($H/r \sim 1$) for the global solutions.

3.5 Parameter space for global and self-similar solutions

In this section, we put effort to determine the Φ_s that admits global accretion solutions for a given set of input parameters (ε_0, ℓ_0, α). Upon tuning the (ε_0, ℓ_0), we compute the maximum value of saturation constant Φ_s^{max} for a given α and present the obtained results in Fig. 5. Here, open circles, open squares, and open asterisks are for $\ell_0 = 2.55$, 2.75, and 3.05 and these points join using solid (blue), dotted (maroon), and dashed (red) lines corresponds to the results for $\varepsilon_0 = 0.0010$, 0.0025, and 0.0050, respectively. We observe that for a set of (ε_0, ℓ_0), Φ_s^{max} increases with the increase of α, which is in agreement with the results obtained from self-similar solutions (Ghasemnezhad et al. 2012; Faghei 2012a). Further, we notice that for a given ε_0, when ℓ_0 is small (high), the flow with relatively higher (lower) viscosity admits global transonic solutions. On the other hand, for a given α, when ε_0 is increased (decreased), the acceptable range of Φ_s^{max} is also increased (decreased), irrespective to the choice of ℓ_0 values. The shaded (violet) region corresponds to the self-similar solutions (see equation 26) where slanting solid line refers the limiting value of saturation constant ($\Phi_s^{max} = \Phi_{sc}$). Here, we choose $f = 1$ and $\gamma = 1.5$. When $\Phi_s > \Phi_s^{max}$, the global solutions become infeasible and ceases to exist (see Section 3.4). It is noteworthy that for lower ℓ_0, Φ_{sc} agrees well with Φ_s^{max} obtained from the global solutions. When ℓ_0 is higher, a coarse agreement is observed for flows with lower ε_0 values. With this, we argue that the physically motivated global accretion solutions are prevalent than the simplistic self-similar solutions.

Next, we compare the limiting range of $\Phi_s^{max} = \Phi_{sc}$ as a function of viscosity parameter α for different γ values. The obtained results are shown in Fig. 6, where Φ_s^{max} is plotted as a function of α. In the figure, the effective domain shaded in violet is for $\gamma = 1.5$, whereas the same in red is obtained for $\gamma = 1.6$. It is evident that the acceptable range of the saturation constant Φ_s decreases as γ is increased (see also Tanaka & Menou 2006). Based on these findings, we infer that self-similar solutions obtained using relatively lower γ seems to be potentially more viable in articulating the features of global accretion solutions of HAFs (see Fig. 5).

3.6 Bernoulli parameter

In this section, we study the Bernoulli parameter *Be* (see equation (18)) which coarsely accounts the evidence of outflow likely to be originated from the accretion disc. Accordingly, in Fig. 7, we display the typical variation of Bernoulli parameter *Be* as a function of radial coordinate (r). In the figure, thick curves correspond to the results obtained from the global accretion solutions, where input parameters are chosen as $\gamma = 1.5, f = 1.0, \alpha = 0.05, \varepsilon_0 = 0.0025$, and $\ell_0 = 2.75$. Here, the solid (black), dashed (red), and dot-dashed (green) curves represent results corresponding to $\Phi_s = 0.0$, 0.0005, and 0.0010. Note that the overall profile of *Be* is in agreement with the smooth solutions reported in Das et al. (2009; see also Kumar & Gu 2018). We find that the Bernoulli parameter *Be* of global transonic solutions remain positive throughout the disc which is again in agreement with Narayan et al. (1997). The positive Bernoulli parameter suggests that the accreting gas are unbound and therefore, a part of the accreting gas may escape (equivalently mass-loss) in the form of outflow with a net positive (kinetic) energy avoiding the strong gravitational pull of the BH. With this, the accreting gas tends to become energetically bound. However, these outflows are expected to be quite weak as the terminal Lorentz factor ranges $\Gamma = Be + 1 \sim 1.01$ (Das et al. 2009). Indeed, shock-induced global accretion solutions seems potentially promising to generate powerful outflows having $\Gamma \sim 6$ (Das et al. 2009); however, implementation of the shock physics is beyond the scope of the present paper and will be reported elsewhere.

It is worthy to compare the Bernoulli parameter obtained from the global and self-similar solutions. Although the Bernoulli parameter of the global transonic solution always remain positive, however,

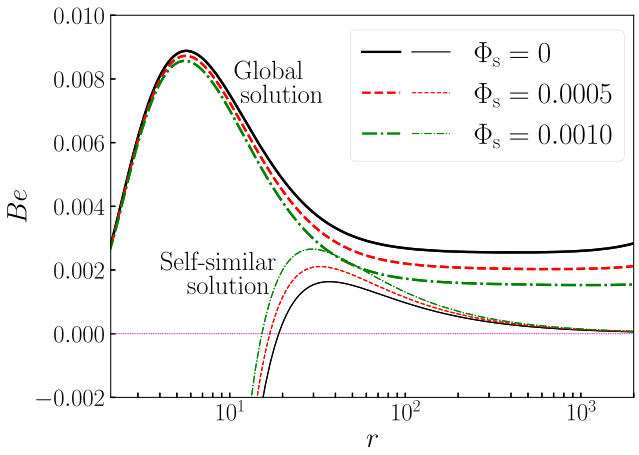

Figure 7. Plot of Bernoulli parameter (*Be*) as a function of radial coordinate for different values of the saturation constant Φ_s. Here, we choose the input parameters as $\gamma = 1.5, f = 1.0$, and $\alpha = 0.05$. Thick curves represent results obtained from the global solutions using $\varepsilon_0 = 0.0025$, and $\ell_0 = 2.75$, whereas thin curves are for the self-similar solutions. The solid (black), dashed (red), and dot–dashed (green) curves denote results for $\Phi_s = 0$, 0.0005, and 0.0010, respectively. The dotted (magenta) horizontal line corresponds to $Be = 0$. See text for the details.

in the self-similar approach, it often alters its sign from positive to negative as the accreting flow moves towards the BH from the outer edge. In Fig. 7, we present the profile of *Be* obtained from the self-similar solutions using thin curves, where $\gamma = 1.5, f = 1.0$, $\alpha = 0.05$ are used as input parameters. As before, the results plotted using the solid (black), dashed (red), and dot–dashed (green) curves are for $\Phi_s = 0.0$, 0.0005, and 0.0010, respectively. We observe that *Be* becomes negative only at the inner part of the disc, where the potential energy overcomes the remaining terms in equation (18) yielding strongly bound flow. This happens because the radial and rotational velocities close to the BH in the self-similar solutions are smaller than those in the global solutions. Further, we notice that the effect of thermal conduction on the Bernoulli parameter *Be* is seen to be opposite. We infer that this finding possibly arises as the radial dependence of the disc variables in the self-similar solutions (see equations 19−21) differs considerably from the global solutions when the thermal conduction is active inside the HAFs.

4 SUMMARY AND DISCUSSION

In this paper, we present a comprehensive study of a low angular momentum steady axisymmetric viscous advective accretion flow around a non-rotating BH in the presence of thermal conduction. Here, the conductive heat flux is described in the saturated form. This is because, the accretion flow becomes weakly collisional in such systems (Quataert 2004; Tanaka & Menou 2006). We adopt the pseudo-Newtonian potential introduced by Paczyński & Wiita (1980) that satisfactorily mimics the space–time geometry around the non-rotating BHs. With this, we examine the effect of thermal conduction on the properties of the global transonic HAFs around BHs.

The present model is based on the same set of governing equations that describes the advection dominated accretion flow (Narayan et al. 1997). Moreover, the conservation equations augmented by the inner boundary conditions (Becker & Le 2003; Das et al. 2009; Kumar & Gu 2018) permit us to carry out the analysis from the location just out side the BH horizon $r_{in} = 2.001$. Using the model input parameters, namely energy (ε_0), angular momentum (ℓ_0), viscosity parameter (α), adiabatic index (γ), and saturation constant (Φ_s), and following the solution methodology presented in Appendix A, we obtain the complete set of global transonic solutions for the first time to the best of our knowledge in the presence of thermal conduction. We summarize our findings below.

We find that the effect of thermal conduction on the global accretion solutions is significant particularly towards the outer part of the disc. When the saturation constant Φ_s exceeds its limiting value, the nature of the global solution is altered and it becomes closed failing to connect the BH horizon with the outer edge of the disc (see Fig. 1). Solution of this kind remains unphysical unless it is connected via shock with another solution passing through a critical point usually located far from the horizon (Fukue 1987; Chakrabarti 1996; Das et al. 2001, 2009, 2022; Chakrabarti & Das 2004; Becker et al. 2008, and references therein). Needless to mention that the studying shock-induced global accretion solution is beyond the scope of this paper and hence, will be reported elsewhere. Moreover, our results confirm that the thermal conduction affects the transonic properties of the HAFs. When Φ_s is increased for flows with fixed input parameters ($\varepsilon_0, \ell_0, \alpha$), critical points recede away from the BH horizon (see Fig. 2).

We also examine the role of thermal conduction in the flow variables. We see that the increase of Φ_s reduces the flow temperature and the disc height at the outer region (see Fig. 3). This possibly happens due to the fact that high thermal conduction generally weakens the viscous turbulence (Faghei 2012a) that lowers the disc temperature. Indeed, these findings are in agreement with the results reported in Tanaka & Menou (2006) and Wu et al. (2010). Further, we compare the flow variables obtained by means of global and self-similar solutions and ample disagreement is seen (see Fig. 4). In fact, we observe that the radial velocity and the sound speed are not noticeably affected by thermal conduction for the self-similar solutions. Notice that the global accretion solutions remain sub-Keperian all throughout, however, self-similar solutions may become super-Keplerian near the critical radius provided α assumes lower value (Chen et al. 1997; Narayan et al. 1997; Kumar & Gu 2018).

One of the important results of this work is to identify the correlation between the viscosity parameter α and the maximum saturation constant Φ_s^{max} that renders the global transonic solutions of HAFs. We find a positive correlation where Φ_s^{max} increases with α irrespective to the choice of (ε_0, ℓ_0). We also observe that the flow with higher ε_0 can sustain higher Φ_s^{max} for the global solutions, however, such dependencies are non-existence indicating the limitation of the self-similar approach (see Fig. 5).

In addition, we calculate the Bernoulli parameter *Be* in the presence of thermal conduction to explore the possible existence of outflows in HAFs. The global solutions display a positive Bernoulli parameter at all radii, whereas the self-similar solutions yield negative Bernoulli parameter at the inner part of the disc (see Fig. 7). Evidently, an accretion flow with positive Bernoulli parameter is unbound and therefore, matter is likely to escape from such unbound disc avoiding the strong gravity of the BH in the from of outflow.

Finally, we mention the limitations of the present formalism as it is developed based on several approximations. We adopt pseudo potential to mimic the gravitational effect around a non-rotating BH, instead of using general relativity. We consider single temperature disc assuming strong coupling existed between ion and electron. However, in HAFs, the ion–electron coupling generally becomes weak and hence, two-temperature flow structure seems to be viable at least at the inner part of the disc (Rees et al. 1982; Yuan & Narayan 2014; Dihingia, Das & Mandal 2018; Dihingia et al.

2020). We neglect magnetic fields although the transport of angular momentum is expected due to the Maxwell stress associated with magnetohydrodynamics turbulence driven by magneto-rotational instability. Moreover, we refrain studying self-consistent accretion-ejection solutions that requires two-dimensional approach. All these are indeed relevant, however, their implementations are beyond the scope of the present work. Indeed, we plan to take up these issues in our future works and will be reported elsewhere.

ACKNOWLEDGEMENTS

Authors thank the anonymous reviewer for valuable comments and useful suggestions that help to improve the quality of the paper. Authors acknowledge the Sci-HPC Center of the Ferdowsi University of Mashhad, where a part of this research is performed. Amin Mosallanezhad is supported by The National Natural Science Foundation of China (grant no. 12150410308), Xi'an JiaoTong University (grant no. QN2022170006L), and the China Postdoctoral Science Foundation (grant no. 2020M673371). Amin Mosallanezhad acknowledges the support of Dr X. D. Zhang at the Network Information Center of Xi'an JiaoTong University. The computation work is done using the High Performance Computing (HPC) platform of Xi'an JiaoTong University. Samik Mitra acknowledges Prime Minister's Research Fellowship (PMRF), Government of India for financial support. Samik Mitra is indebted to Mr Amit Kumar for valuable suggestions. Santabrata Das thanks Science and Engineering Research Board (SERB), India for support under grant MTR/2020/000331. Samik Mitra and Santabrata Das also thank the Department of Physics, IIT Guwahati, India for providing the facilities to complete this work. Authors also acknowledge the extensive use of the NASA Astrophysical Data System Abstract Service.

DATA AVAILABILITY

The data underlying this article will be available with reasonable request.

REFERENCES

Abramowicz M. A., Zurek W. H., 1981, ApJ, 246, 314
Abramowicz M. A., Czerny B., Lasota J. P., Szuszkiewicz E., 1988, ApJ, 332, 646
Abramowicz M. A., Chen X. M., Granath M., Lasota J. P., 1996, ApJ, 471, 762
Abramowicz M. A., Lasota J.-P., Igumenshchev I. V., 2000, MNRAS, 314, 775
Aktar R., Das S., Nandi A., 2015, MNRAS, 453, 3414
Aktar R., Das S., Nandi A., Sreehari H., 2017, MNRAS, 471, 4806
Aktar R., Das S., Nandi A., Sreehari H., 2018, JA&A, 39, 17
Becker P. A., Le T., 2003, ApJ, 588, 408
Becker P. A., Das S., Le T., 2008, ApJ, 677, L93
Bu D.-F., Yang X.-H., 2019, ApJ, 871, 138
Bu D.-F., Yuan F., Stone J. M., 2011, MNRAS, 413, 2808
Bu D.-F., Wu M.-C., Yuan Y.-F., 2016a, MNRAS, 459, 746
Bu D.-F., Yuan F., Gan Z.-M., Yang X.-H., 2016b, ApJ, 818, 83
Bu D.-F., Yuan F., Gan Z.-M., Yang X.-H., 2016c, ApJ, 823, 90
Chakrabarti S. K., 1989, ApJ, 347, 365
Chakrabarti S. K., 1996, ApJ, 464, 664
Chakrabarti S. K., Das S., 2004, MNRAS, 349, 649
Chatterjee K. et al., 2020, MNRAS, 499, 362
Chen L.-H., Wang J.-M., 2004, ApJ, 614, 101
Chen X., Abramowicz M. A., Lasota J.-P., 1997, ApJ, 476, 61
Cheung E. et al., 2016, Nature, 533, 504
Cowie L. L., McKee C. F., 1977, ApJ, 211, 135
Das S., 2007, MNRAS, 376, 1659
Das S., Chattopadhyay I., 2008, New A, 13, 549
Das S., Chattopadhyay I., Nandi A., Chakrabarti S. K., 2001, A&A, 379, 683
Das S., Becker P. A., Le T., 2009, ApJ, 702, 649
Das S., Nandi A., Stalin C. S., Rakshit S., Dihingia I. K., Singh S., Aktar R., Mitra S., 2022, MNRAS, 514, 1940
Davis S. W., Done C., Blaes O. M., 2006, ApJ, 647, 525
Dexter J., Quataert E., 2012, MNRAS, 426, L71
Dihingia I. K., Das S., Mandal S., 2018, MNRAS, 475, 2164
Dihingia I. K., Das S., Prabhakar G., Mandal S., 2020, MNRAS, 496, 3043
Esin A. A., McClintock J. E., Narayan R., 1997, ApJ, 489, 865
Faghei K., 2012a, Ap&SS, 338, 301
Faghei K., 2012b, MNRAS, 420, 118
Frank J., King A., Raine D. J., 2002, Accretion Power in Astrophysics, 3rd edn. Cambridge Univ. Press, Cambridge, p. 398
Fryer C. L., Woosley S. E., Hartmann D. H., 1999, ApJ, 526, 152
Fukue J., 1987, PASJ, 39, 309
Ghasemnezhad M., Khajavi M., Abbassi S., 2012, ApJ, 750, 57
Ghoreyshi S. M., Shadmehri M., 2020, MNRAS, 493, 5107
Godet O. et al., 2012, ApJ, 752, 34
Haba Y., Terashima Y., Kunieda H., Ohsuga K., 2008, PASJ, 60, 487
Hameury J. M., Lasota J. P., McClintock J. E., Narayan R., 1997, ApJ, 489, 234
Homan J., Neilsen J., Allen J. L., Chakrabarty D., Fender R., Fridriksson J. K., Remillard R. A., Schulz N., 2016, ApJ, 830, L5
Ichimaru S., 1977, ApJ, 214, 840
Johnson B. M., Quataert E., 2007, ApJ, 660, 1273
Khajenabi F., Shadmehri M., 2013, MNRAS, 436, 2666
Kumar R., Gu W.-M., 2018, ApJ, 860, 114
Kumar R., Yuan Y.-F., 2021, ApJ, 910, 9
Lamb D. Q., Lamb F. K., Pines D., 1973, Nat. Phys. Sci., 246, 52
Lasota J. P., Abramowicz M. A., Chen X., Krolik J., Narayan R., Yi I., 1996, ApJ, 462, 142
Liang E. P. T., Thompson K. A., 1980, ApJ, 240, 271
Liu B. F., Done C., Taam R. E., 2011, ApJ, 726, 10
Liu J. Y., Liu B. F., Qiao E. L., Mineshige S., 2012, ApJ, 754, 81
Lu J.-F., Gu W.-M., Yuan F., 1999, ApJ, 523, 340
Ma R.-Y., Roberts S. R., Li Y.-P., Wang Q. D., 2019, MNRAS, 483, 5614
Mahadevan R., Quataert E., 1997, ApJ, 490, 605
Manmoto T., Mineshige S., Kusunose M., 1997, ApJ, 489, 791
Meyer F., Liu B. F., Meyer-Hofmeister E., 2000, A&A, 354, L67
Mineshige S., Kawaguchi T., Takeuchi M., Hayashida K., 2000, PASJ, 52, 499
Mitra S., Maity D., Dihingia I. K., Das S., 2022, MNRAS, 516, 5092
Mosallanezhad A., Zeraatgari F. Z., Mei L., Bu D.-F., 2021, ApJ, 909, 140
Mosallanezhad A., Bu D.-F., Čemeljić M., Zeraatgari F. Z., Hai Y., Mei L., 2022, ApJ, 939, 12
Nakamura K. E., 1998, PASJ, 50, L11
Nakamura K. E., Kusunose M., Matsumoto R., Kato S., 1997, PASJ, 49, 503
Narayan R., Fabian A. C., 2011, MNRAS, 415, 3721
Narayan R., Yi I., 1994, ApJ, 428, L13
Narayan R., Yi I., 1995a, ApJ, 444, 231
Narayan R., Yi I., 1995b, ApJ, 452, 710
Narayan R., Kato S., Honma F., 1997, ApJ, 476, 49
Nemmen R. S., Storchi-Bergmann T., Yuan F., Eracleous M., Terashima Y., Wilson A. S., 2006, ApJ, 643, 652
Nemmen R. S., Storchi-Bergmann T., Eracleous M., 2014, MNRAS, 438, 2804
Netzer H., Trakhtenbrot B., 2014, MNRAS, 438, 672
Ohsuga K., Mineshige S., Mori M., Kato Y., 2009, PASJ, 61, L7
Paczyński B., Wiita P. J., 1980, A&A, 500, 203
Park J., Hada K., Kino M., Nakamura M., Ro H., Trippe S., 2019, ApJ, 871, 257
Popham R., Gammie C. F., 1998, ApJ, 504, 419
Quataert E., 2004, ApJ, 613, 322
Quataert E., 2008, ApJ, 673, 758

Rees M. J., Begelman M. C., Blandford R. D., Phinney E. S., 1982, Nature, 295, 17
Reynolds C. S., Di Matteo T., Fabian A. C., Hwang U., Canizares C. R., 1996, MNRAS, 283, L111
Sarkar B., Das S., Mandal S., 2018, MNRAS, 473, 2415
Shadmehri M., 2008, Ap&SS, 317, 201
Shakura N. I., Sunyaev R. A., 1973, A&A, 24, 337
Soria R., Kuntz K. D., Long K. S., Blair W. P., Plucinsky P. P., Winkler P. F., 2015, ApJ, 799, 140
Tanaka T., Menou K., 2006, ApJ, 649, 345
Treves A., Belloni T., Bouchet P., Chiappetti L., Falomo R., Maraschi L., Tanzi E. G., 1988, ApJ, 335, 142
Veledina A., Poutanen J., Vurm I., 2013, MNRAS, 430, 3196
Wang J. M., Netzer H., 2003, A&A, 398, 927
Wang Q. D. et al., 2013, Science, 341, 981
Watarai K.-y., Mizuno T., Mineshige S., 2001, ApJ, 549, L77
Weinberg S., 1972, Gravitation and Cosmology: Principles and Applications of the General Theory of Relativity. Wiley VCH, New York, p. 688
Wilkinson T., Uttley P., 2009, MNRAS, 397, 666
Wu M., Yuan F., Bu D., 2010, Sci. China Phys. Mech. Astron., 53, 168
Yang H., Yuan F., Yuan Y.-F., White C. J., 2021, ApJ, 914, 131
Younes G., Ptak A., Ho L. C., Xie F.-G., Terasima Y., Yuan F., Huppenkothen D., Yukita M., 2019, ApJ, 870, 73
Yuan F., 1999, ApJ, 521, L55
Yuan F., Cui W., 2005, ApJ, 629, 408
Yuan F., Narayan R., 2014, ARA&A, 52, 529
Yuan F., Markoff S., Falcke H., 2002, A&A, 383, 854
Yuan F., Ma R., Narayan R., 2008, ApJ, 679, 984
Yuan W., Liu B. F., Zhou H., Wang T. G., 2010, ApJ, 723, 508
Yuan F., Wu M., Bu D., 2012a, ApJ, 761, 129
Yuan F., Bu D., Wu M., 2012b, ApJ, 761, 130
Yuan F., Gan Z., Narayan R., Sadowski A., Bu D., Bai X.-N., 2015, ApJ, 804, 101
Yuan F., Yoon D., Li Y.-P., Gan Z.-M., Ho L. C., Guo F., 2018, ApJ, 857, 121

APPENDIX A: SOLUTION METHODOLOGY: ITERATION METHOD

We obtain the global transonic solutions using an iteration method. In this method, we begin the numerical integration of the flow equations from a location just outside the BH horizon as $r_{\rm in} = r_{\rm s} + 0.001$. For a given set of input parameters (ε_0, ℓ_0, α, $\Phi_{\rm s}$), we compute three flow variables, namely velocity $v_{\rm in}$, sound speed $C_{s_{\rm in}}$, and angular momentum $\ell_{\rm in}$ at $r_{\rm in}$. Needless to mention that $0 < \ell_0 < \ell_{\rm ms}$, where $\ell_{\rm ms} = 2\sqrt{3}$ is the innermost stable angular momentum around a Schwarzschild BH. Considering this, we pursue the following chronology for obtaining the global solutions.

(i) Close to the horizon i.e. $r - r_{\rm s} \rightarrow 0$, the matter falls with free fall velocity $v_{\rm ff} = -\sqrt{2/(r - r_{\rm s})}$. Here, we consider a fractional constant $\delta < 1$, such that $v_{\rm in} = \delta \times v_{\rm ff}$, and the accreting matter enters into the BH with this velocity $v_{\rm in}$.

(ii) Next, we determine the asymptotic flow variables just outside the horizon at $r_{\rm in}$. Using Frobenius expansion, we get the asymptotic behaviour of flow angular momentum as,

$$\ell_{\rm in} = \ell_0 + B(r - r_{\rm s})^{\beta}; \qquad r \rightarrow r_{\rm s}, \tag{A1}$$

where B and β are positive constants. We implement $\ell_{\rm in}$ in equation (8) and we demand that,

$$\lim_{r\rightarrow r_{\rm s}} \frac{{\rm d}\ell_{\rm in}}{{\rm d}r} = 0, \qquad \lim_{r\rightarrow r_{\rm s}} \frac{\delta\sqrt{2}B(r - r_{\rm s})^{\beta}}{\sqrt{r_{\rm s}}(r - r_{\rm s})^{\frac{3}{2}}\alpha C_{\rm s}^2} = \frac{2\ell_0}{r_{\rm s}}. \tag{A2}$$

To eliminate all terms involving $(r - r_{\rm s})$ in equation (A2), we require $\beta = 3/2$ and $B = \sqrt{2/r_{\rm s}}(\alpha C_{\rm s}^2 \ell_0/\delta)$. Accordingly, we get the expression of angular momentum at $r_{\rm in}$ for a suitable choice of (δ, ℓ_0, α, $\Phi_{\rm s}$).

(iii) We use $v_{\rm in}$ and $\ell_{\rm in}$ in equation (16), where we consider that the effect of conduction is negligible (Tanaka & Menou 2006), and determine the sound speed $C_{s_{\rm in}}$ by solving equation (17) for a given energy ε_0,

(iv) Using $v_{\rm in}$, $C_{s_{\rm in}}$, and $\ell_{\rm in}$, we start integrating equations (8, 10, 11) from $r_{\rm in}$ outwards, and check the critical point conditions described in equations (12) and (13). We keep tuning the iteration parameter δ until the critical point conditions are satisfied for $\delta = \delta_{\rm c}$, and thereafter, we obtain the critical point $r_{\rm c}$ (see Fig. A1 for more details).

(v) At $r_{\rm c}$, we calculate ${\rm d}v/{\rm d}r|_{\rm c}$ by applying the L$'$Hôpital's rule. The real and negative radial velocity gradient corresponds to accretion solution, and hence, for ${\rm d}v/{\rm d}r|_c < 0$, we further integrate equations (8, 10, 11) starting from $r_{\rm c}$ upto to the outer edge of the disc $r_{\rm edge} = 1000$. Finally, we join both parts of the solutions (from $r_{\rm in}$ to $r_{\rm c}$ and $r_{\rm c}$ to $r_{\rm edge}$) to obtain the global transonic accretion solution for a HAF around a non-rotating BH.

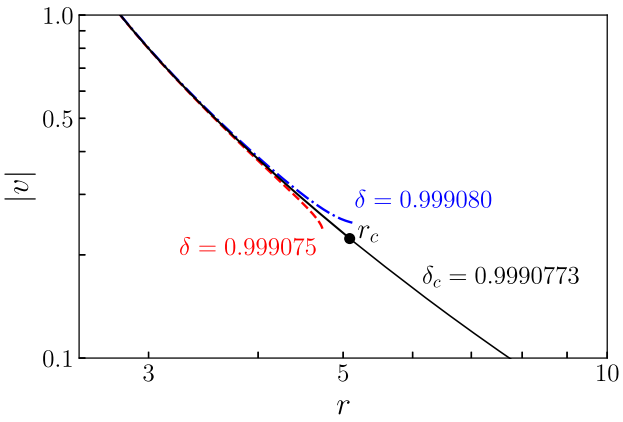

Figure A1. Variation of flow velocity $|v|$ as a function of radial coordinate r for three different iteration parameters. The dashed (red), solid (black), and dot–dashed (blue) curves denote the results for $\delta = 0.999\,075$, $0.999\,0773$, and 0.999080. Here, $\delta = \delta_{\ c} = 0.999\,0773$ corresponds to the transonic solution where critical point is obtained at $r_{\rm c} = 5.0286$ for the chosen input parameters $(\varepsilon_0, \ell_0, \alpha, \Phi_{\rm s}, \gamma) = (0.005, 3.05, 0.04, 0.0015, 1.5)$.

This paper has been typeset from a TEX/LATEX file prepared by the author.